Egypt.J.Chem. **Vol. 63,** No. 2 pp.483-498 (2020)

Egyptian Journal of Chemistry
http://ejchem.journals.ekb.eg/

Adsorption of Methylene Blue Dye on Hydrothermally Prepared Tungsten Oxide Nanosheets

A. S. Doma*, **Nazly Hassan, A. I. Abd El-Hamid and Hesham M. A. Soliman**
Advanced Technology and New Materials Research Institute (ATNMRI), City of Scientific Research and Technological Applications (SRTA-City), New Borg El-Arab City, 21934 Alexandria, Egypt.

METHYLENE blue (MB) dye was successfully adsorbed on hydrothermally prepared tungsten oxide (WO_3) nanosheets. Scanning electron microscopy (SEM), X-ray diffraction (XRD), Fourier transform infrared (FTIR) and energy-dispersive X-ray spectroscopy (EDS) were used to characterize the prepared powder. Different parameters affecting the adsorption process were investigated such as, contact time, tungsten oxide dose, MB concentration, pH and temperature. In order to detect the kinetic of adsorption process, first, second-order kinetics and intra-particle diffusion models were considered. The second-order model exhibited the best description of MB adsorption onto $WO_3.H_2O$. Adsorption equilibrium data obtained from Langmuir, Freundlich and Tempkin isotherm models showed that the dye uptake is a chemisorption process and the dye species prefer to adsorb on the $WO_3.H_2O$ surface as a monolayer with adsorption capacity Q^o = 13.33 mg g^{-1}. Thermodynamic data revealed that the adsorption reaction is exothermic and spontaneous. The effect of different crystalline phases of tungsten oxide nanosheets was also investigated. The hydrated form ($WO_3 \cdot H_2O$) nanosheets (orthorhombic)showed higher adsorption performance than the non-hydrated structure WO_3 nanosheets (monoclinic).

Keywords: Tungsten oxide; methylene blue; hydrothermal; nanosheets.

Introduction

Water pollution is a serious issue that is expected to worsen over the coming decades. Some organic compounds such as dyes are not biodegradable or bio-transformable and hence persist in the environment for a long time. Industrial dye effluents, resulting from different products such as: paper, plastics, leather, pharmaceutical, food, cosmetics, dyestuffs and textiles, have always been a serious environmental problem [1]. Methyl blue (MB) is one of the most common dyes, which is widely used as coloring agent and disinfector in dye stuffs, rubbers, pharmaceuticals, pesticides and varnishes [1].

Therefore, removal of such pollutants from water is important to protect the environment. Among the various methods available for water purification, adsorption is a fast, inexpensive and widely applicable technique. Several adsorbents have been investigated to remove MB from aqueous solutions such as, graphene oxide [2], composite [3-5], clay [6], adsorption waste [7], activated carbons [8, 9], pyrolytic tire char [10] and palygorskite [11].

Metal oxide nanoparticles exemplify low cost, easy to produce and chemically stable materials. Tungsten oxide (WO_3) is an interesting transition metal oxide that used in wide-range of applications such as; Photocatalysis [12, 13] electrocatalysis [14], Li-ion batteries [15], Electrochromic [16], thermochromic [17] and photochromic devices [18]. WO_3 nanoparticles have been successfully synthesis with different morphologies e.g. nanoneedles [19] or nanofibers

* Corresponding author: ahmed_egypt25@yahoo.com
Recevied 2/11/2019 , accepted 21/1/2020.
DOI: 10.21608/ejchem.2020.18997.2171

[20], nanowire [21- 23], nanorods [24], nanoplates [25] and nanosheets [26]. Several techniques were investigated for preparation of tungsten oxide nanostructures, among of them pulsed spray pyrolyzed [16], anodization [27], arc discharge [28], pulsed laser deposition [29], precipitation [30] and hydrothermal method [30-32].

The hydrothermal method, in which the heat of the feed liquid (usually water) is rising up to its supercritical state and the hydrothermal synthesis reaction, occurred in the supercritical water. Under the hydrothermal condition the properties of the feed change drastically around the critical point and therefore the equilibrium and speed of reactions in used liquid also change greatly. Consequently, the phase state also remarkably changes with the property changes and it forms a uniform phase with the gas which make a suitable environment for growth of the crystals. So, the obtained nanoparticles were found to be as a single crystalline in most cases and had smaller particle size compared with those synthesized under the subcritical conditions. This technique used to synthesis large number of compounds such as complex oxides, tungstates, molybdates, carbonates, silicates, etc. The hydrothermal synthesis appears to be wide applicable method this is referring to the capability of this technique to synthesis not only the fine metal oxide particles of a single component but also the composite of mixed material, less complicated, low temperature and cost-effectiveness efficient tool for the synthesis of anisotropic nanoscale materials

Herein, an easy hydrothermal route is reported for preparation WO_3 nanosheets (two crystalline structure of WO_3 were prepared; hydrated form $WO_3.H_2O$ (orthorhombic) and non-hydrated form WO_3 (monoclinic)). The acidification step of Na_2WO_4 was carried out using suitable ion exchange resin to produce H_2WO_4 species which is the building unit of WO_3 nanosheets. Moreover, the hydrated form $WO_3.H_2O$ shows a good adsorptive capability towards the cationic organic dyes in water.

Experimental

Materials

Sodium tungstate dehydrate ($Na_2WO_4 \cdot {}^2H_2O$, > 98%) from Sigma-Aldrich. Strong HCl acid (type of cation exchange resin) were obtained from Merck. All the adsorption experiments were done using distilled water.

Preparation of Ion-Exchange Resin Column

A plastic column with height of 10.0 cm and diameter 2.8 cm was filled with 50g of the cation exchange resin. Before the using of ion exchange resin, 50 mL of doubly distilled water was introduced to move through the column to clean the resin.

Preparation of Tungsten Oxide Nanostructure

In a typically experiment, a schematic diagram of the different experimental stages is seen in (Fig. 1a-c), a solution of Na_2WO_4 (0.5M) was prepared by dissolving a certain amount of $Na_2WO_4 \cdot {}^2H_2O$ salt with 10 mL deionized water. The packed column was filled with the prepared solution. Fig. 1a demonstrates that the yellow solution was recovered from the column by elution process. The solution could charge onto a stainless-steel autoclave cell and aged at 50°C in a muffle for 24 h. After that, the autoclave cell left to cool to room temperature in air (Fig. 1b). The obtained yellow powder was collected by centrifugation and washed 5 times with distilled water and finally it was dried at 70 °C. Additionally, a part of the collected powder was annealed at 350°C for one hour in air, Fig. 1c.

Characterizations

The morphology was determined by scanning electron microscopy (SEM; JSM 6360LA, Japan). The crystal structure of the samples was specified by X-ray diffraction (XRD; Shimadzu XRD-6100). Fourier transform infrared (FT-IR) analysis was done using Shimadzu FTIR (Model, FTIR-8400, Japan) to depict the functional groups of the sorbent. The elemental analysis of the sorbent before and after the adsorption process was done by the EDS unit related to SEM.

Adsorption Studies

Typically, the tested MB dyes was prepared by dissolving 1.0 g of the dye powder in 1L double distilled water to organize a solution of (1000 mg/L) of MB and desired concentrations were prepared with further dilution. Batch experiments were investigated in50 mL glass beaker contains 10 mL of dye solution with different doses of the nanopowder composite in the range (5–50 mg) were used as adsorbents for each adsorption test. Definite initial concentrations ranged from (50, 100, 150, 200 mg/L) of MB dye solution were prepared. The initial pH of dye solution, ranged from 2.0 to 6.0, was appropriated using 0.1 M NaOH and HCl solutions. The temperature was varied from 25 to 80 °C. The samples were collected by centrifugation and the concentration

of the remaining dye species was detected at 662 nm using UV/Vis. Spectrophotometer-Double beam (T80+, PG instruments Ltd., UK.). The dye removal percent (R%) is defined as given formula (Eq. (1)):

$$R\ \% = \frac{C_o - C_e}{C_o} \times 100 \quad (1)$$

where C_0 and C_e are the initial and equilibrium concentrations of the liquid phase of the dye (mg/L), respectively.

Mathematical Modeling

Adsorption Kinetics; Pseudo first order kinetic is given by Lagergren equation [33], Eq.2:

$$\log(q_e - q_t) = \log q_e + \frac{K_{ads}\, t}{2.303} \quad (2)$$

q_t is the amount of solute sorbed per mass of sorbent (mg/ g) at any time, q_e is the amount of sorption at equilibrium time and K_{ads} (min^{-1}) is the rate constant of pseudo first order sorption.

$$q_e = \frac{(C_o - C_e)v}{1000w} \quad (3)$$

v is the volume of dye solution (mL) and w is the dry weight of the adsorbent (g) and

$$q_t = \frac{(C_o - C_t)v}{1000w} \quad (4)$$

where C_t is the concentration of the dye (mg/L) at different time intervals. A pseudo second order kinetic model is explained by ***Ho*** equation [34], Eq.5.

$$\frac{t}{q_t} = \frac{1}{K_2 q_e^2} + \frac{t}{q_e} \quad (5)$$

where K_2 is the pseudo second order rate constant (g $mg^{-1}min^{-1}$).

Weber–Morris Intra-Particle Diffusion Plot

The kinetic results have been developed by using the Intra-particle diffusion model. This model has been developed by Weber and Morris

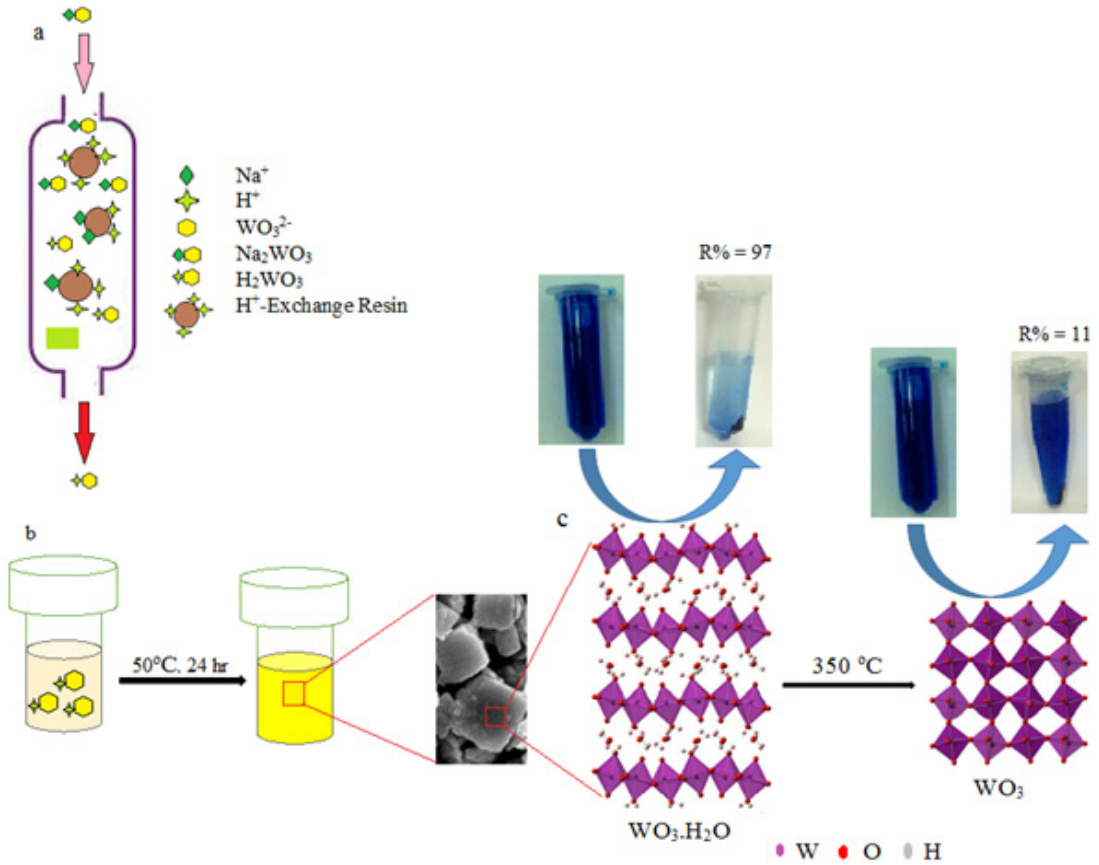

Fig. 1. Schematic diagram illustrated various experimental steps: a) ion exchange step of Na2WO4•2H2O, b) hydrothermal process of H2WO4, c) depiction of atomic structure of hydrated (WO3.H2O) form and its conversation into anhydrous structure (WO3) and d) the dye removal by using the two different structure

[35]. The initial rate of intra-particle diffusion is calculated from the linearization of equation. The sorption process is directly proportional to the square root of the contact time as follows in Eq.6.

$$q_t = k_i t^{0.5} + C \quad (6)$$

where K_i is the intra-particle diffusion rate constant (mg g^{-1} $min^{-1/2}$), C is the intercept and q_t is the amount of dye adsorbed (mg g^{-1}).

Isotherm Models

The adsorption isotherm is very helpful to represent how the adsorbed molecules spread between the liquid and the solid phases when the adsorption process achieves an equilibrium state. Adsorption isotherm were investigated by the three most applied models; Langmuir, Freundlich and Tempkin models. The parameters obtained from the models give important information about the sorption mechanism, the surface property and affinity of the adsorbent. The isotherm models are stated as follows:

Langmuir isotherm supposes that the surface contains homogeneous binding sites, equivalent sorption energies and no interaction between the adsorbed variables. Its mathematical form is established as in Eq. 7:

$$\frac{C_e}{q_e} = \frac{1}{Q^0 b} + \left(\frac{1}{Q^0}\right) C_e \quad (7)$$

where Q^0 is the monolayer adsorption capacity (mg/g), b is a constant concerning the free energy of adsorption, q_e is the equilibrium adsorption capacity (mg g^{-1}). A plot of C_e/q_e versus C_e gives a straight line where Q^0 and b are two parameters which are determined from the slope and the intercept, respectively.

Freundlich isotherm is an empirical equation based on an exponential distribution of adsorption sites and energies. It is represented as in Eq. 8;

$$log\ q_e = log k_f + \frac{1}{n}\ log\ C_e \quad (8)$$

where K_f (mg/g) and n are the Freundlich exponents, related to adsorption capacity and adsorption intensity, respectively. Therefore, a linear plot of log q_e versus log C_e determines the Freundlich exponents and also prove the reliability of the Freundlich model.

Tempkin isotherm model is supposing a directly proportional between the sorption process is to the square root of the contact time as presented in the following equation Linear form of Tempkin isotherm model is expressed by Eq. 9;

$$q_e = B_1 LnA_1 + B_1 LnC_e \quad (9)$$

where B_1 is the constant related to heat of sorption and A_1 (L/mg) is the Tempkin equilibrium isotherm constant.

Thermodynamic Model

For the calculation of thermodynamic parameters, the subsequent equations were used:

$$K_c = \frac{C_{ad}}{C_e} \quad (10)$$

$$\Delta G^0 = -RT LnK_c \quad (11)$$

$$LnK_c = \frac{\Delta S^0}{R} - \frac{\Delta H^0}{RT} \quad (12)$$

where K_c is the equilibrium constant, C_e is the equilibrium concentration in solution (mg/L) and C_{ad} is the amount adsorbed on the adsorbent (mg/L) at equilibrium.D$G°$, D$H°$ and $\Delta S°$are changes in Gibbs free energy (kJ/mol), enthalpy change (kJ/mol) and entropy change (J.mol/K), respectively. R is the gas constant (8.314 J/mol K) and T is the absolute temperature (K).

Results and Discussion

Characterization

The morphology of as-prepared $WO_3 \cdot H_2O$ at different magnification is presented in SEM micrographs, Fig.2a- b. From the SEM images $WO_3 \cdot H_2O$ appears as a nanosheets structure with a heterogeneous size and dimensions as seen in Fig. 2c. This plate form confirmed its layered crystal structure. The as-prepared tungsten oxide (hydrated form, $WO_3 \cdot H_2O$) was annealed at 350°C in air for 1 h to give (non-hydrated form, WO_3). The XRD of the two forms ($WO_3 \cdot H_2O$ and WO_3) are shown in Fig. 3.

The FTIR spectra of $WO_3.H_2O$, MB and $WO_3.H_2O$/MB complex were presented in Fig.4. From the IR spectrum of $WO_3.H_2O$, Fig.4, the intense broad band at 3406 cm^{-1} revealed the stretching motion of (O-H), the medium narrow band at 1616 cm^{-1} is characteristic of in-plane bending δ (H-O-H) of the water molecule. A very intense broad band in the region 902-621cm^{-1} corresponding to different motion arising from W-O linkage. Therefore, the band at 902 cm^{-1} refers to the stretching of (W=O_t) (where O_t the terminal oxygen). The bands at 763 cm^{-1} and 694 cm^{-1} revealed the stretching (W-O) and the band at 713 cm^{-1} is due to stretching (W-O-W) [36]. The bands characteristic to MB-dye are showed in Fig. 4. Additionally, after adsorption of MB over WO_3, the $WO_3.H_2O$/MB complex is created and

its IR spectrum is given in Fig. 4. In comparison between the three IR spectrum of $WO_3.H_2O$, MB and $WO_3.H_2O$/MB complex, we can detect that there is a shift in different bands for both MB and $WO_3.H_2O$ and $WO_3.H_2O$/MB complex. In contract, for MB the benzene ring stretching band at 1597 cm^{-1} (Fig.4) is shifted to 1624 cm^{-1} (Fig. 4) and the symmetric deformation of $–CH_3$ at 1350 cm^{-1} (Fig.4) is shifted to 1388 cm^{-1} (Fig. 4) [37]. Furthermore, the stretching bands at 902, 763 and 663 cm^{-1} of $WO_3.H_2O$ (Fig. 4) are shifted to 912, 798 and 663 cm^{-1}, respectively (Fig. 4), this is attributed to the interaction between the $WO_3.H_2O$ and MB-dye [38].

EDAX analysis shows that the prepared $WO_3.H_2O$ is very pure as shown in Fig.5. The prepared powder is mainly composed of %At (W = 30.58 and O = 69.42) this percent around the stoichiometric composition of WO_3. After treating the contaminated water of MB by $WO_3.H_2O$, the EDAX analysis showed the presence of carbon, as revealed in Fig.5, denoting an interaction between MB and $WO_3.H_2O$.

Adsorption Equilibrium Studies

Effect of Contact Time

The effect of contact time on the removal percent (%R) of MB-dye at $WO_3.H_2O$ dose 50 mg, [MB] 100 ppm, pH 7 and T 25 °C is observed in Fig. 6. However, from Fig. 6, the adsorption of MB-dye by $WO_3.H_2O$ is simultaneously occurred, where 97% of the dye was removed within 1 min. After that the adsorption percent becomes constant for almost 1 hr. Therefore, 1 minute was selected as contact time for other experimental parameters.

Adsorption Kinetics

The mostly famous two models used to analyze the adsorption process are the pseudo first and second order kinetic, which are shown in Figs. 6b & c, respectively. The fitting parameters of experimental data obtained by using the linear equations (2& 5) are reported in Table1. The value of the correlation coefficient, , of the pseudo second order is 0.999 and the calculated q_e value equals (10.03 mg g^{-1}) is more near to the experimental value. This suggests that the

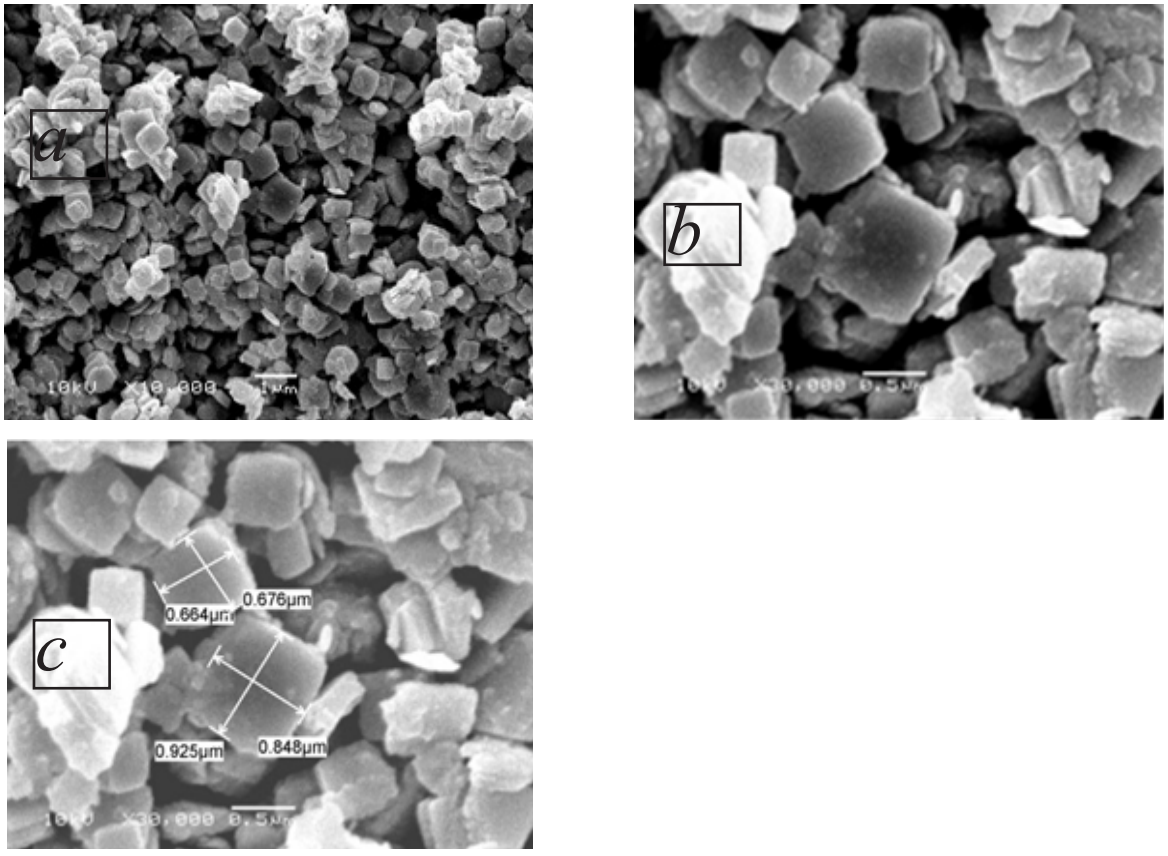

Fig. 2. SEM micrograph of as-prepared tungsten oxide at different magnifications

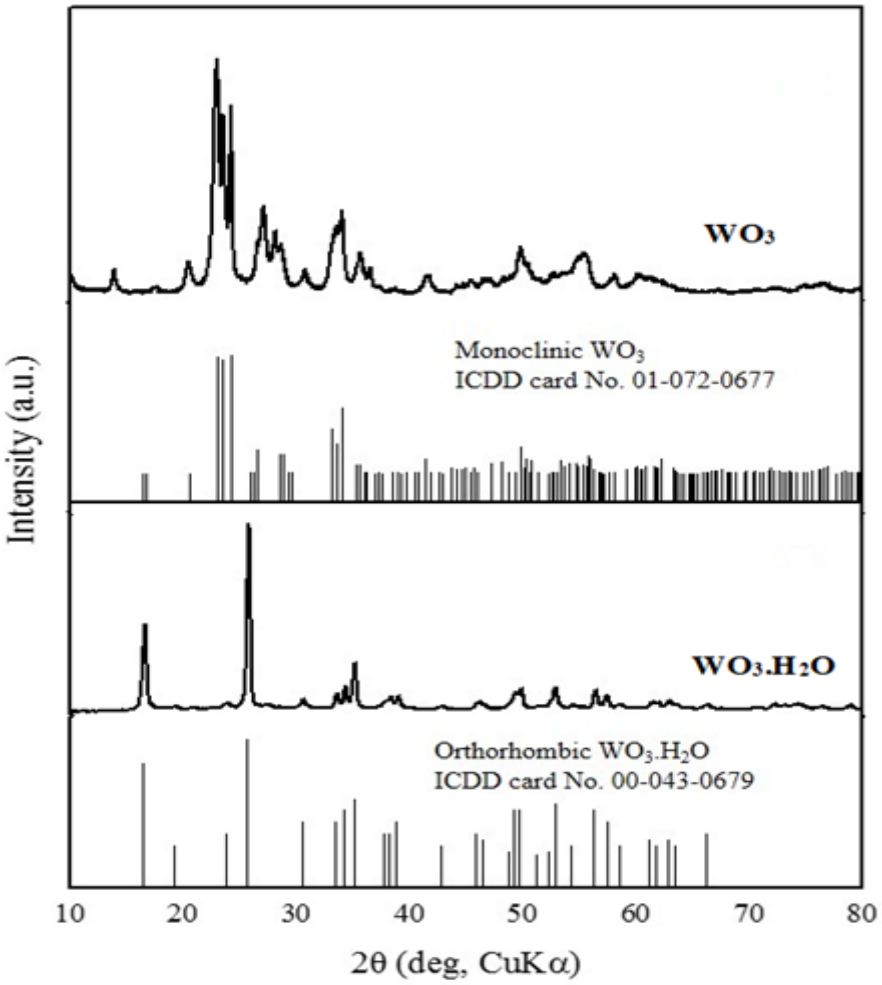

Fig. 3. XRD pattern of as-prepared tungsten oxide sample (WO3.H2O) and after annealing at 350 °C in air for 1 h (WO3).

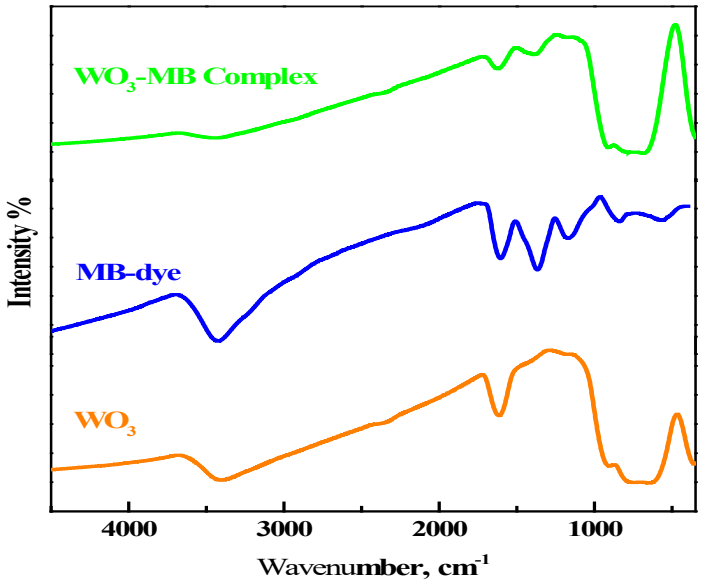

Fig. 4. FTIR spectra of a) tungsten oxide, b) MB and c) complex of MB and tungsten oxide.

adsorption of methylene blue on the nanoplates follow the second-order kinetics. The q_t values are plotted against $t^{0.5}$ (according to Eq. 6), the obtained straight line does not pass into the origin. From the obtained results (Fig. 6d), it is clear that the intra particle diffusion is not the only rate dominant process in this system.

The Effect of $WO_3.H_2O$ Dose

The removal percent () of MB-dye improved from 12 to 97% as $WO_3.H_2O$ dose increased from 5 mg to 50 mg as indicated in Fig. 7. This may refer to the fact that as the dose of the $WO_3.H_2O$ increases, larger surface area and more adsorption sites are created resulting in removal of higher number of MB-dye molecules [39, 40].

The Effect of the Initial Dye Concentration

Apparently, as the initial concentration of MB-dye increases, lowering in the removal percent (R%) takes place. In this study, 50-200 ppm MB-dye was tested and a reduction in the removal percent (%R) was recorded, as shown in Fig.8a. This may be attributed to as more sites in the substrate are filled; it becomes more difficult for the MB-dye molecules to fit onto an available vacant site. Moreover, the adsorbed molecules are more likely to adsorb as a monolayer on a surface containing a finite number of identical sites [41].

Adsorption Isotherm

Adsorption isotherm is a most powerful way to report how solutes interact with adsorbents and it is essential to optimize the use of these adsorbents. Some adsorption models are considered for the MB-dye adsorption such as Langmuir, Freundlich and Tempkin isotherms.

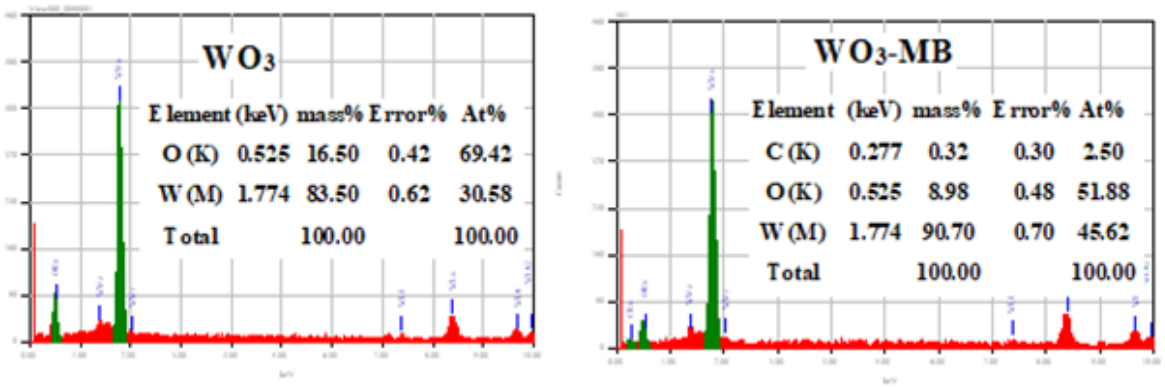

Fig. 5. EDAX analysis of a) tungsten oxide and b) complex of MB and tungsten oxide.

TABLE 1. Calculated parameters of pseudo first order and pseudo second order kinetic models

Adsorbent / Parameter		MB
q_{eexp} (mg g^{-1})		9.95
First-order kinetic parameter	K_1 (min^{-1}) q_{ecal} (mg g^{-1}) R^2	-1.460 3.800 0.890
Second-order kinetic parameter	K_2 (g $mg^{-1}min^{-1}$) q_{ecal}(mg g^{-1}) R^2	1.530 10.030 0.999
Intra-particle diffusion	k_i (mg g^{-1} $min^{-0.5}$) C R^2	3.730 5.680 0.940

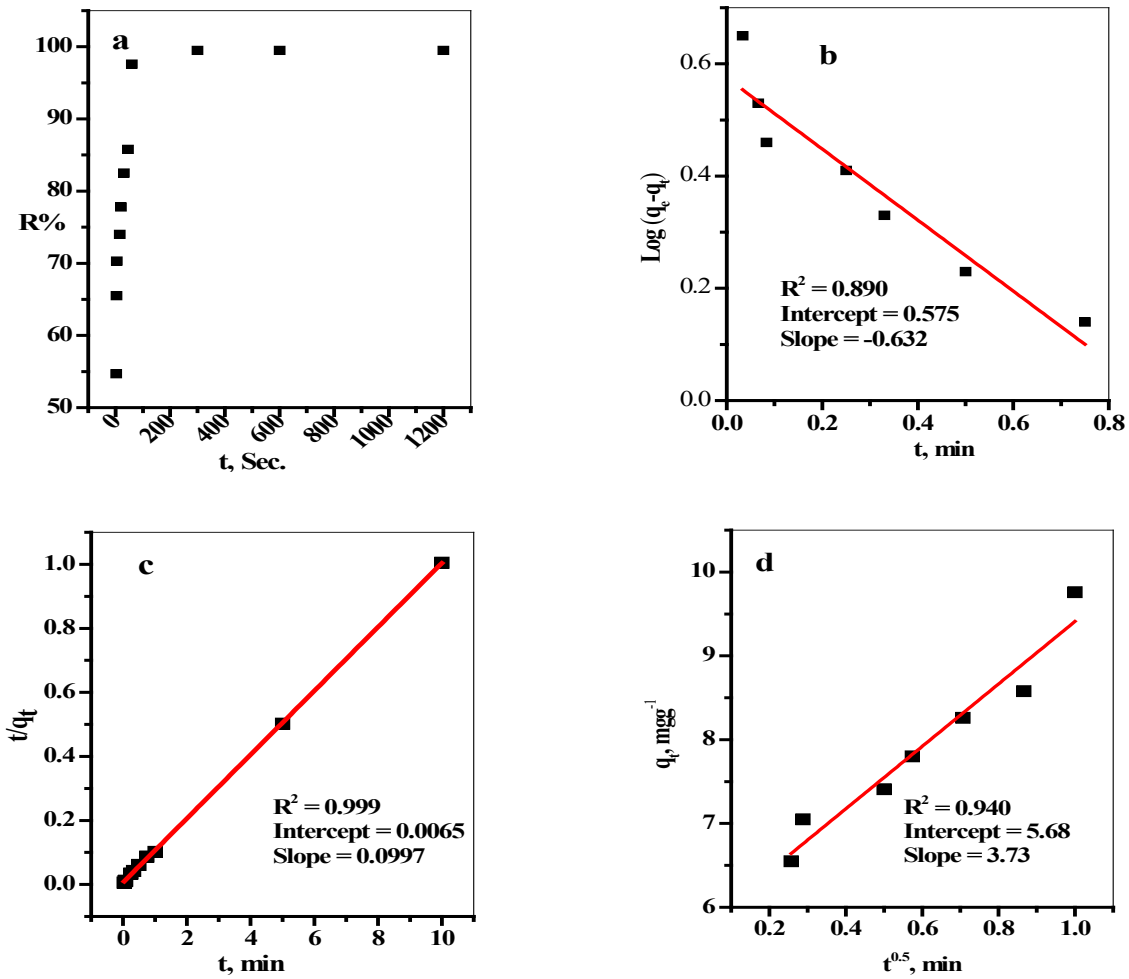

Fig.6. a) Effect of the contact time on the removal percent (R%) of MB-dye from aqueous solution by WO3.H2O, b) Lagergreen plots, c) Pseudo second-order plot and d) Weber–Morris intra-particle diffusion plot for the adsorption of MB using WO3.H2O.

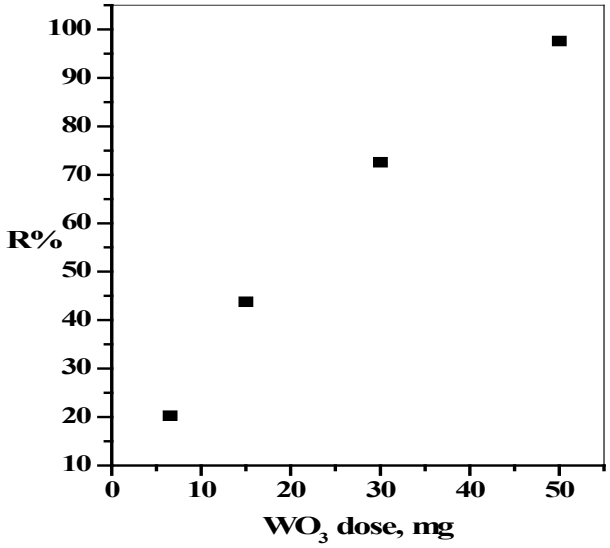

Fig. 7. Effect of WO3.H2O dose on the removal percent (R%) of MB-dye from aqueous solution. (Time = 1 min, [MB] = 100 ppm, pH = 7 and T = 25 oC)

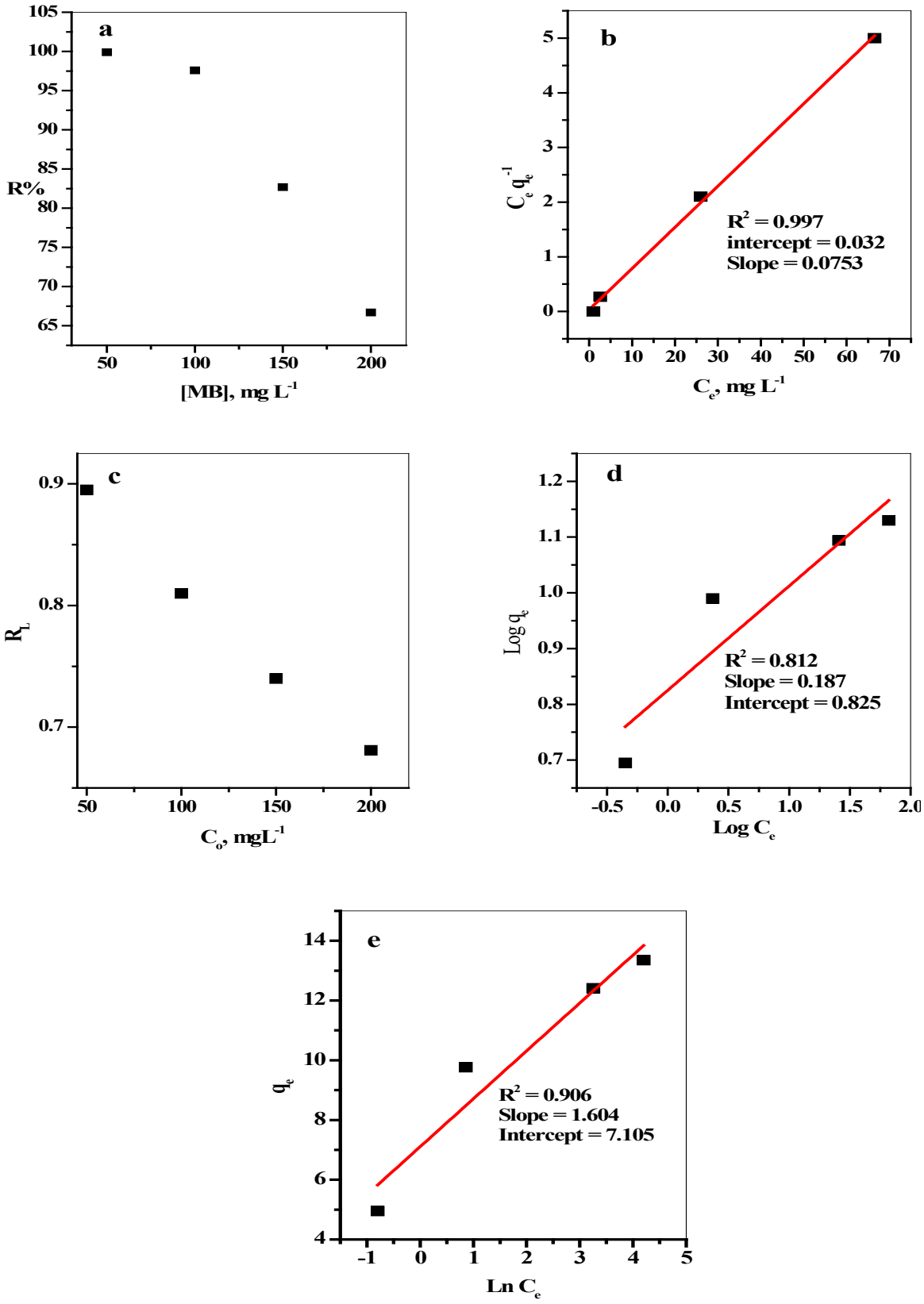

Fig. 8. a) Effect of the initial MB concentration on the removal percent (R%)of MB-dye from aqueous solution by WO3.H2O, b) Langmuir, c) dimensionless separation factor, RL, d) Freundlich, e) Tempkin adsorption isotherm of methylene blue on WO3.H2O (Time = 1 min, WO3 dose = 50 mg, pH = 7 and T = 25 oC).

Langmuir Isotherm Model

Langmuir isotherm assumes a monolayer adsorption onto a surface containing a finite number of uniform adsorption sites with no transmigration of adsorbate in the surface plane. The adsorption isotherm was investigated according to the linear form of Langmuir model using Eq. 7. The linear plots of the regression equations are shown in Fig. 8b and the regression coefficients (R^2) are recorded in Table 2. As detected, the resulted value of R^2 is 0.98, which explains why Langmuir model is suitable to fit with adsorption process of methyl blue dye onto WO_3 that indicating the chemisorptions process.

According to the results of the Langmuir isotherm shown in Table 2, The value of R_L which describes the shape of the isotherm is given be (Eq.13):

$$R_L = \frac{1}{1+bC_0} \quad (13)$$

where R_L should be $0 < R_L < 1$. The type of the isotherm depends on R_L values. If $R_L > 1$ the isotherm is unfavorable, if R_L equals 1 that means linear isotherm, for $R_L < 1$ the isotherm is favorable and when $R_L = 0$ it is irreversible. The significance value of R_L is setbetween0.895 and 0.681 as in Fig. 8c. This assumed that the $WO_3.H_2O$ is suitable for adsorption of MB dye under these conditions.

Freundlich Isotherm Model

Freundlich isotherm model assumes heterogeneous surface energies, in which the energy term in Langmuir equation varies as a function of the surface coverage. Adsorption isotherms were examined using the linear form of Freundlich model using Eq. 3. The linear regression is presented in Fig. 8d. The regression coefficient (R^2), k_f and n_f are calculated and displayed in Table 2. The value of $1/n_f$ is less than unity indicating that the adsorption occurs at low concentration, while the amount of adsorbed molecules became lowest at the highest concentration.

Tempkin Isotherm Model

The adsorption data for MB on $WO_3.H_2O$ were analyzed referring the Tempkin isotherm model Eq. 9 and the linear regression is plotted in Fig. 8e. The correlation coefficient (= 0.906) shows the poorest fit to the experimental adsorption equilibrium data, as summarized in Table 2.

The Effect of Solution pH

The charges on the adsorbent surface and the degree of adsorption are highly affected by the pH of the solution. Fig. 9 shows the relation between the pH in the range (2-6) and *R*% of MB-dye. It is clear that the dye removal percent increases by increasing pH or by lowering H^+ concentration this is due to the increase the negativity of nanoparticles. This manner will be lead to increase the electrostatic attraction between the nanoparticles and the positively charged dye species. On the other hand, at low pH, the concentration of $[H^+]$ is high and the H-ion will be more competitive the cationic dye species on the adsorbed active sites of WO_3 NPs.

The Effect of Temperature

The physical bonding between the dye molecules and the active sites of $WO_3.H_2O$ nanostructure becomes weaker by raising the

TABLE 2. Parameters of Langmuir, Freundlich and Tempkin adsorption isotherm models for MB adsorbed by $WO_3.H_2O$.

Isotherm models	Parameter	Value
Langmuir	Q^o (mg g^{-1}) b (mg^{-1}) R^2	13.330 2.34 x 10^{-3} 0.980
Freundlich	K_f (mg g^{-1}) 1/n R^2	6.683 0.187 0.812
Tempkin	B_1 A_1 R^2	1.604 2.6 x 10^4 0.906

temperature that results in lowering *R*%. Fig.10a, shows that *R*% decreases with increasing the temperature from 25 ℃ to 80 ℃. In addition, the solubility of the dye molecules increases, thus the interaction between the dye molecules and the solvent becomes stronger than that between the dye molecules and the sorbent [42].

Thermodynamic Study

The studies of thermodynamics have been applied to estimate the spontaneity of the adsorptive process. The thermodynamic parameters values for the adsorption of MB on WO_3. H_2O at different temperatures were computed and listed in Table 3. The Gibbs free energy change ($\Delta G°$) was estimated using Eq. 11, also the values of ($\Delta H°$) and ($\Delta S°$) have been calculated from the slope and intercept of the relation of ln K_c versus 1/T using Eq. 12. From the data of Fig. 10b, the values of ($\Delta G°$) are negative showing that the sorption of MB-dye on $WO_3.H_2O$ is an instantaneous process. The negative value of enthalpy change $\Delta H°$ is a further confirm for the exothermic nature of the process and the negative entropy $\Delta S°$ reflects the affinity of the adsorbent material toward the dye molecules (Table 3).

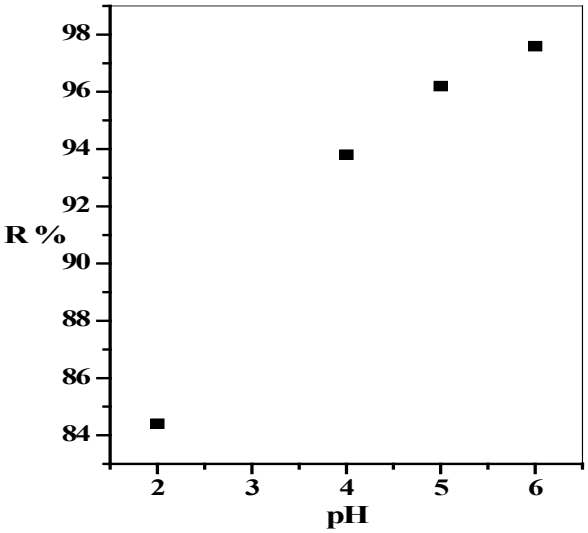

Fig. 9. Effect of pH on the removal percent (R%) of MB-dye from aqueous solution by WO3.H2O. (Time = 1 min, WO3 dose = 50 mg, [MB] = 100 ppm and T = 25 oC)

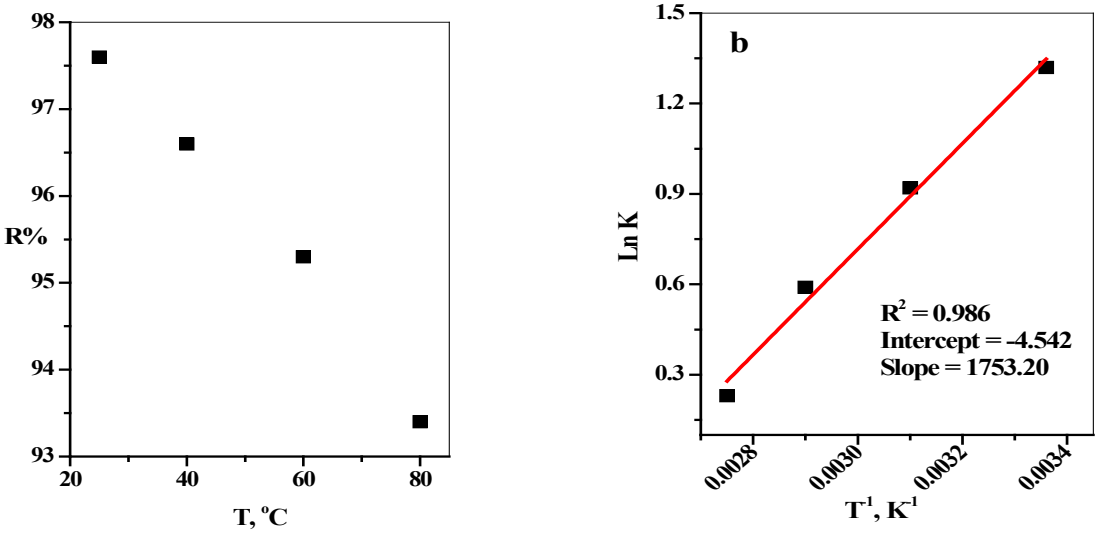

Fig.10. a) Effect of the temperature on the removal percent (R%) of MB-dye from aqueous solution by WO3.H2O and b) Plot of ln K versus T-1 for sorption of MB by WO3.H2O. (Time = 1 min, WO3.H2O dose = 50 mg, [MB] = 100 ppm and pH = 7)

The optimum conditions of our experiment (Time = 1 min, solid dose = 50 mg, [MB] = 100 ppm, pH = 7 and T = 25 °C) were applied using the other crystal structure of tungsten oxide (non-hydrated form, WO_3, refers to Fig. 1c). The experimental results illustrate that the phase transferring (from the hydrated form $WO_3.H_2O$ to non-hydrated WO_3 crystal structures) leads to a decrease in *R*% from 97% to 11%, respectively, as in Fig. 11a. This may be attributed to the terminal oxygen atoms presented in the hydrated structure$WO_3.H_2O$ that are ‘‘unsteady state atoms”. As a consequence, the unsteady state oxygen atoms interact with nitrogen atoms in MB molecules leading to a rapid adsorption of MB [36]. In addition, the presence of the interlayer H_2O molecules in the hydrated form increases the adsorption by the electrostatic attraction between the O-atom lone pair of the interlayer H_2O molecules and the positive charge of N-atom of MB molecule. The detailed explanation is schematically illustrated in Fig. 11b. While annealing at 350°C, the phase will be transferred from orthorhombic to monoclinic. This transformation consumed the terminal oxygen ($W=O_t$) in the formation of W-O-W network structure and this may decrease the activity of the new structure.

The Maximum MB molecule uptake capacity, given by in Langmuir model, was 13.33 mgg^{-1}, Table 2. Identical values of MB adsorption on other adsorbents obtained from the literature are demonstrated in Table 4. The Adsorption capacity is minimal in this study compared to some adsorbent. However, this result does not reduce the probability of using $WO_3.H_2O$ as adsorbents for MB abstraction from aqueous solutions, since it displays suitable adsorption capacity comparing to the other.

TABLE 3. Thermodynamic parameters for MB sorption by $WO_3.H_2O$.

T, (K)	ΔG° (kJ/mole)	ΔH° (kJ/mole)	ΔS° (kJ/mole)
298	-3.27	-0.55	-210.85
323	-2.47		
343	-1.68		
363	-0.69		

TABLE 4. Langmuir based maximum adsorption capacity of several adsorbents for MB adsorption.

Adsorbent	Q, mg g^{-1}	References
Natural zeolite	23.60	43
NZVI/ZSM	20.88	44
Modified pumice stone	15.87	45
$WO_3.H_2O$	13.33	This study
Melamine—Urea resin	12.10	46
Raw beech sawdust	9.78	47
Guava seeds activated carbon	6.50	48
Coir pith activated carbon	5.78	49
Posidoniaoceanica (L.) fibres	5.60	50
Fly ash	5.57	51
Neem leaf powder	3.76	52

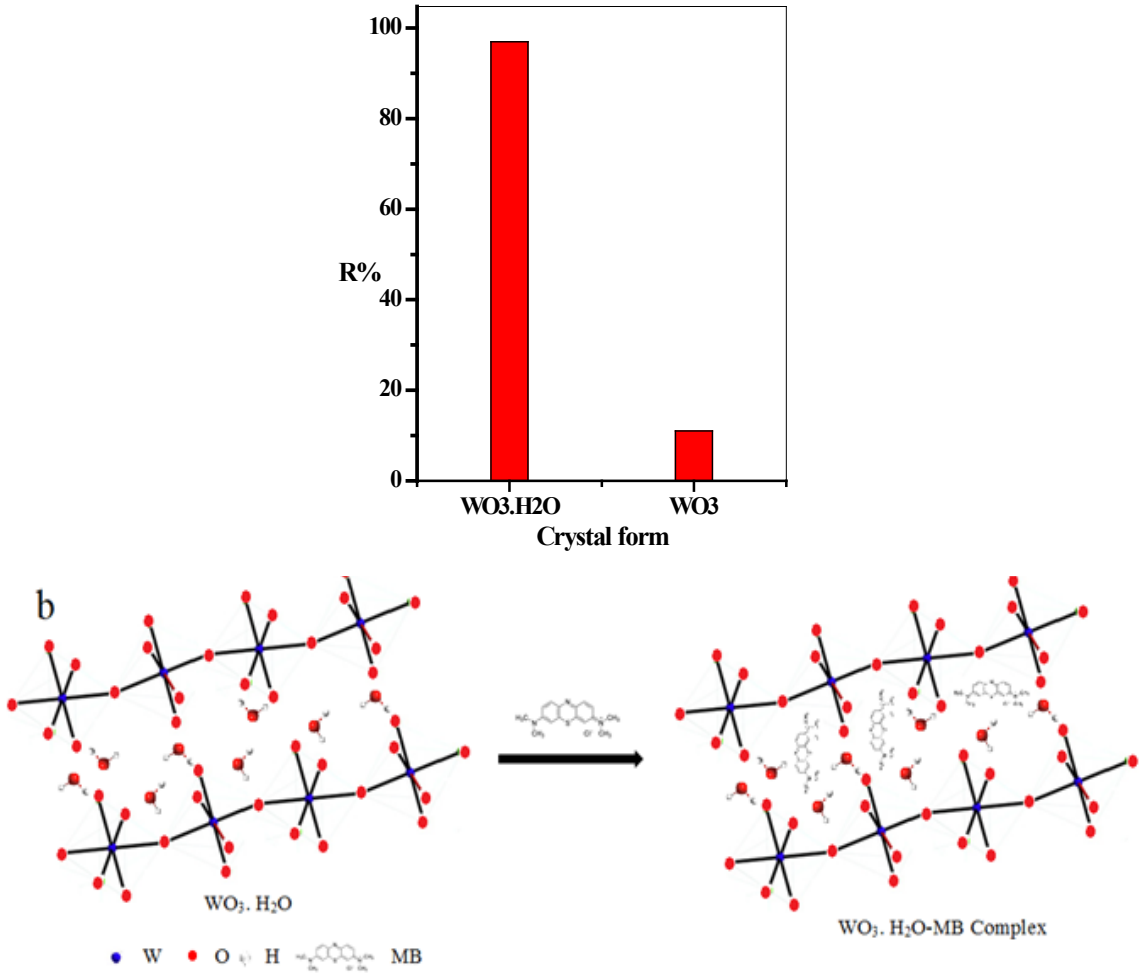

Fig. 11. a) Comparison between the R% for both hydrated (WO3.H2O) and non-hydrated (WO3) structure and b) Schematic illustration of the proposed "adsorption-mechanism'' of WO3.H2O to MB.

Conclusion

Experiments indicated that hydrothermally prepared tungsten oxide nanosheets are suitable for the sorption of methylene blue dye from aqueous media. Adsorption kinetics was well fitted by pseudo-second order kinetic model equation. The adsorption equilibrium was better described by Langmuir model in comparison to both Freundlich and Tempkin models. The thermodynamic parameters present that the adsorption process is spontaneous and exothermic. Additionally, the data reflect the affinity of the adsorbent material toward the dye molecules. The hydrated structure $WO_3.H_2O$ possesses a better adsorption than anhydrous WO_3. This study exhibits $WO_3.H_2O$ as an inexpensive and easily prepared adsorbent for the removal of cationic dyes in aqueous media treatments.

References

1. Fan Z., Jing L., Ye Y., Tiefeng W., RuiqZ in T., Weijie S., Adsorption behavior and mechaa nism of methyl blue on zinc oxide nanoparticles, J Nanopart Res. 15, 2034-2043(2013).

2. Abd-Elhamid A.I., Aly H.F, Soliman H.A.M., El-Shanshory A. A., Graphene oxide: Follow the oxidation mechanism and its application in water treatment, J.Mol. Liq. 265, 226–237(2018).

3. Abd-Elhamid A.I., Kamoun E.A., El-Shanshory A.A., Soliman H.M.A, Aly H.F., Evaluation of graphene oxide-activated carbon as effective composite adsorbent toward the removal of cationic dyes: Composite preparation, characterization and adsorption parameters, J. Mol. Liq. 279, 530–539(2019).

4. Abd-Elhamid A.I., Nayl A.A., El. Shanshory A.A., *Egypt. J. Chem.* **63**, No.2(2020)

Soliman H.M.A., Aly H. F., Decontamination of organic pollutants from aqueous media using cotton fiber–graphene oxide composite, utilizing batch and filter adsorption techniques: a comparative study, RSC Adv., 9, 5770–5785 (2019).

5. Nayl A.A., Abd-Elhamid A.I., El-Shanshory A.A., Soliman H.M.A., Kenawy E.-R., Aly H.F., Development of sponge/ graphene oxide composite as eco-friendly filter to remove methylene blue from aqueous media, Appl. Surf. Sci., 496, 143676(2019).

6. Abd-Elhamid A.I., El Fawal G.F., AklM.A., Methylene Blue and Crystal Violet Dyes Removal (As A Binary System) from Aqueous Solution Using Local Soil Clay: Kinetics Study and Equilibrium Isotherms, *Egypt. J. Chem.* 62(3), 941 - 954 (2019).

7. **Abd-Elhamid A.I., Aly H.F., Removal of Fe (III) from Aqueous Solution Using Thiosalcylic Acid as an Efficient and Novel Adsorbent,** *Egypt.J.Chem.,* 61(4), 617- 627 (2018).

8. Jian Z., Yan Z., Meiyan J., Juan L., Jiawei S., Removal of methylene blue from aqueous solution by adsorption on pyrophyllite, J. Mol. Liq. 209, 267–271(2015).

9. Abd-Elhamid A.I., Doma A.S., El-SyedA.M., Kenawy E.-R., Eco-friendly activation of charcoal for purification of water from colored organic pollutants, *Res.* J. Chem. Environ., 23 (3), 83-95(2019).

10. Vasiliki M., Aris G., Yiannis D., Ioannis K., Adsorption of phenol and methylene blue from aqueous solutions by pyrolytic tire char: Equilibrium and kinetic studies, J. Environ. Chem. Eng.3, 574–582(2015).

11. Wang W., Tian G., Zhang Z., Wang A., A simple hydrothermal approach to modify palygorskite for high-efficient adsorption of Methylene blue and Cu(II) ions, Chem. Engin. J. 265, 228–238(2015).

12. Sadakane M, Sasaki K, Kunioku H, Ohtani B, Ueda W, Abe R., Preparation of nano-structured crystalline tungsten (vi) oxide and enhanced photocatalytic activity for decomposition of organic compounds under visible light irradiation., Chem Commun (Camb). 28 (48), 6552-4(2008). doi: 10.1039/b815214d.

13. Kominami H., Yabutani K. I., Yamamoto T., Kera Y., Ohtani B., Synthesis of highly active tungsten (VI) oxide photocatalysts for oxygen evolution by hydrothermal treatment of aqueous tungstic acid solutions, J. Mater. Chem.11, 3222-3227 (2001).

14. Xiangzhi C., Limin G., Fangming C., Qianjun H.,Jianlin S., Electrocatalytic Activity and CO Tolerance Properties of Mesostructured Pt/WO_3 Composite as an Anode Catalyst for PEMFCs, J. Phys. Chem. C, 113, –٤١٣٤ ٢٠٠٩)٤١٣٨), DOI: ١٠,١٠٢١/jp٨٠٧٩٢٠٥.

15. Kai H., Qingtao P., Feng Y., Shibing N., Xiucheng W., Deyan H., Controllable synthesis of hexagonal WO_3 nanostructures and their application in lithium batteries, J. Phys. D: Appl. Phys. 41, 155417(2008), doi:10.1088/0022-3727/41/15/155417.

16. Suvarna R.B., Patil P.S., Electrochromic characteristics of pulsed spray pyrolyzed polycrystalline WO_3 thin films, Smart Mater. Struct. 18, 025004 (2009).

17. Alamri S.N., Study of thermocolored WO_3 thin film under direct solar radiation, Smart Mater. Struct. 18, 025010(2009).

18. Luo Z., Yang J., Cai H., Li H., Ren X., Liu J., Liang X., Preparation of silane-WO_3 film through sol–gel method and characterization of photochromism, Thin Solid Films 516, 5541-5544(2008).

19. Gerand B., Nowogrocki G., Guenot J., Figlarz M., Structural study of a new hexagonal form of tungsten trioxide, J. Solid State Chem. 29, 429-434(1979).

20. Lu X., Liu X., Zhang W., Wang C., Wei Y., Large-scale synthesis of tungsten oxide nanofibers by electrospinning, J. Coll..Interf. Sci., 298, 996-999 (2006).

21. Gu Z., Li H., Zhai T., Yang W., Xia Y., Ma Y., Yao J., Large-scale synthesis of single-crystal hexagonal tungsten trioxide nanowires and electrochemical lithium intercalation into the nanocrystals, J. Solid State Chem., 180, 98-105(2007).

22. Song X.C., Zheng Y.F., Yang E., Wang Y., Large-scale hydrothermal synthesis of WO_3 nanowires in the presence of K_2SO_4, Mater. Lett., 61, 3904-3908 (2007).

23. Zhang J., Tu J., Xia X., Wang X. L., Gu C., Hydrothermally synthesized WO_3 nanowire arrays with highly improved electrochromic performance, J. Mater. Chem., 21, 5492-5498(2011).

24. Wang J., Khoo E., Lee P.S., Ma J., Controlled

Synthesis of WO_3 Nanorods and Their Electrochromic Properties in H_2SO_4 Electrolyte, J. Phys. Chem. C 113, 9655-9658 (2009).

25. Ma J., Zhang J., Wang S., Wang T., Lian J., Duan X., Zheng W., Topochemical Preparation of WO_3 Nanoplates through Precursor $H_2WO_4$and Their Gas-Sensing Performances, J. Phys. Chem. C 115, 18157-18163 (2011).

26. Wei X., Wenting L., Xuhui M., Hua Z., Dihua W., Na_2SO_4-assisted synthesis of hexagonal-phase WO3 nanosheet assemblies with applicable electrochromic and adsorption properties, J. Mater. Chem. A 1, 1261-1269 (2013).

27. Mozalev A., Khatko V., Bittencourt C., Hassel A.W., Gorokh G., Llobet E., Correig X., Nanostructured Columnlike Tungsten Oxide Film by Anodizing Al/W/Ti Layers on Si, Chem. Mater., 20, ٦٤٩٣–٦٤٨٢ (2008), DOI: 10.1021/cm801481z.

28. Ashkarran A.A., Irajizad A., Ahadian M.M., Ardakani S.A.M., Synthesis and photocatalytic activity of WO_3 nanoparticles prepared by the arc discharge method in deionized water. Nanotechn., 19, 195709 (2008). doi:10.1088/0957-4484/19/19/195709.

29. Lethy K.J., Beena D., Mahadevan Pillai V.P., Ganesan V., J. Bandgap renormalization in titania modified nanostructured tungsten oxide thin films prepared by pulsed laser deposition technique for solar cell applications, Appl. Phys. 104, 033515-1 - 033515-12 (2008). DOI: 10.1063/1.2953070.

30. Balázsi C., Pfeifer J., Development of tungsten oxide hydrate phases during precipitation, room temperature ripening and hydrothermal treatment, Solid State Ionics 151, 353-358 (2002).

31. Mo R.F., Jin G.Q., Guo X.Y., Morphology evolution of tungsten trioxide nanorods prepared by an additive-free hydrothermal route, Mater. Lett. 61, 3787-3790 (2007).

32. Kominami H., Yabutani K. I., Yamamoto T., Kera Y., Ohtani B., Synthesis of highly active tungsten (VI) oxide photocatalysts for oxygen evolution by hydrothermal treatment of aqueous tungstic acid solutions, J. Mater. Chem. 11, 3222-3227 (2001).

33. Lagergren, S., About the theory of so-called adsorption of soluble substances. K. Sven. Vetenskapsakad. Handlingar Band, 24, 1 – 39 (1898).

34. Ho Y.S. and McKay G., The sorption of lead (II) ions on peat, Water Res., 33, 578 – 584(1999).

35. Vadivelan V., Kumar K.V., Equilibrium, kinetics, mechanism, and process design for the sorption of methylene blue onto rice husk, J. Coll.Interf. Sci. 286, 90-100 (2005).

36. Sharma N., Deepa M., Varshney P., Agnihotry S.A., FTIR investigations of tungsten oxide electrochromic films derived from organically modified peroxotungstic acid precursors, thin solid films 401, 45-51 (2001).

37. Feng W., Chuanhao L., Jimmy C.Y., Hexagonal tungsten trioxide nanorods as a rapid adsorbent for methylene blue, Sep.Puri. Techn. 91, 103–107 (2012).

38. Zhang H.Y., Xu L., Wang E.B., Jiang M., Wu A.G., Li Z., Photochromic behavior and luminescent properties of novel hybrid organic–inorganic film doped with Preyssler'sheteropoly acid $H_{12}[EuP_5W_{30}O_{110}]$ and polyvinylpyrrolidone, Mater. Lett. 57, 1417–1422 (2003).

39. Adriana S.F., Leandro S.O., Mauro E.F., Kinetics and equilibrium studies of methylene blue adsorption by spent coffee grounds, Desalin. 249, 267–272 (2009).

40. Farook A., Lingeswarran M., Radhika T.., Ceria and Titania incorporated silica based catalyst prepared from rice husk: Adsorption and photocatalytic studies of methylene blue, J. Coll. Interf. Sci. 406, 209–216 (2013).

41. Noureddine B., Samir Q., Ali A., Abederrahman N., Yhya A.-I., Removal of Reactive Yellow 84 from aqueous solutions by adsorption onto hydroxyapatite, J. Saudi Chem. Soc. 15, 263–267 (2011).

42. Mansoor A., Samira S., Removal of acid dyes from aqueous media by adsorption onto amino-functionalized nanoporous silica SBA-3, Dyes and Pigments 94, 1-9 (2012).

43. Jafari-zare F., Habibi-yangjeh A., Competitive adsorption of methylene blue and rhodamine B on natural zeolite: thermodynamic and kinetic studies, Chin. J. Chem. 28, 349–356 (2010).

44. Atyaf K. H., Nugroho D., Dongyun D., Mohd H., Rahim M.R.N., Novel modified ZSM-5 as an efficient adsorbent for methylene blue Removal, J. Environ. Chem. Engin. 4, 2607–2616 (2016).

45. Derakhshan Z., Baghapour M., Adsorption

of methylene blue dye from aqueous solutions by modified pumice stone: kinetics and equilibrium studies, Health Scope 2 (3) (2013).

46. Ozdemir F.A., Demirata B., Apak R., Adsorptive removal of methylene blue from simulated dyeing wastewater with melamine-formaldehyde-urea resin, J. Appl. Polym. Sci. 112 (6), 3442–3448 (2009).

47. Batzias F.A., Sidiras D.K., Dye adsorption by calcium chloride treated beech sawdust in batch and fixed-bed systems, J. Hazard. Mater. B114, 167–174 (2004).

48. Rahman I.A., Saad B., Utilization of Guava seeds as a source of activated carbon for removal of methylene blue from aqueous solution, Malaysian J. Chem. 5 (1), 8–14 (2003).

49. Kavitha D., Namasivayam C., Experimental and kinetic studies on methylene blue adsorption by coir pith carbon, Bioresour. Technol. 98, 14–21 (2007).

50. Ncibi M.C., Mahjoub B., Seffen M., Kinetic and equilibrium studies of methylene blue biosorption by Posidonia oceanica (L.) fibres, J. Hazard. Mater. 139, 280–285 (2007).

51. Kumar K.V., Ramamurthi V., Sivanesan S., Modeling the mechanism involved during the sorption of methylene blue onto fly ash, J. Coll. Interf. Sci. 284, 14–21 (2005).

52. Bhattacharyya K.G., Sharma A., Kinetics and thermodynamics of methylene blue adsorption on Neem (Azadirachta indica) leaf powder, Dyes Pigments 65, 51–59(2005).